Sulfur availability regulates plant growth via glucose-TOR signaling

Yihan Dong[1], Marleen Silbermann[1], Anna Speiser[1], Ilaria Forieri[1], Eric Linster[1], Gernot Poschet[1], Arman Allboje Samami[1], Mutsumi Wanatabe[2], Carsten Sticht[3], Aurelio A. Teleman[4], Jean-Marc Deragon[5], Kazuki Saito[2], Rüdiger Hell[1] & Markus Wirtz [1]

Growth of eukaryotic cells is regulated by the target of rapamycin (TOR). The strongest activator of TOR in metazoa is amino acid availability. The established transducers of amino acid sensing to TOR in metazoa are absent in plants. Hence, a fundamental question is how amino acid sensing is achieved in photo-autotrophic organisms. Here we demonstrate that the plant Arabidopsis does not sense the sulfur-containing amino acid cysteine itself, but its biosynthetic precursors. We identify the kinase GCN2 as a sensor of the carbon/nitrogen precursor availability, whereas limitation of the sulfur precursor is transduced to TOR by downregulation of glucose metabolism. The downregulated TOR activity caused decreased translation, lowered meristematic activity, and elevated autophagy. Our results uncover a plant-specific adaptation of TOR function. In concert with GCN2, TOR allows photo-autotrophic eukaryotes to coordinate the fluxes of carbon, nitrogen, and sulfur for efficient cysteine biosynthesis under varying external nutrient supply.

[1] Centre for Organismal Studies (COS), University of Heidelberg, Im Neuenheimer Feld 360, 69120 Heidelberg, Germany. [2] Graduate School of Pharmaceutical Sciences, Chiba University, Chiba, 260-8675, Japan. [3] Center for Medical Research, University of Mannheim, 68167 Mannheim, Germany. [4] German Cancer Research Center (DKFZ), 69120 Heidelberg, Germany. [5] Laboratory of Genomes and Plant Development, Centre National de la Recherche Scientifique, University of Perpignan, 66100 Perpignan, France. Correspondence and requests for materials should be addressed to R.H. (email: ruediger.hell@cos.uni-heidelberg.de) or to M.W. (email: markus.wirtz@cos.uni-heidelberg.de)

Plants continuously decide how to balance the use of their acquired resources for growth or for stress responses, since they must compete with their neighbors for acquisition of nutrients by developmental plasticity and they must fight environmental challenges on site. Protein turnover causes up to 50% of total energy costs in fast growing cells[1]. Consequently, one immediate reaction of cells to various stresses, including nutrient starvation, is translation arrest. This thereby releases energy and resources for stress responses. Besides numerous regulatory events for selective translation and direct modification of the ribosome subunits that affect mRNA binding via the Cap-binding proteins, translation is regulated in eukaryotes frequently via two processes: formation of the translational pre-initiation complex and rRNA transcription for ribosome biogenesis reviewed in refs. [2–4]. Formation of the pre-initiation complex is mainly triggered by phosphorylation of the eukaryotic initiation factor 2α (eIF2α). eIF2α is phosphorylated in mammals by four sensor kinases (GCN2, PERK, PKR, and HRI), which are activated by diverse stresses defining eIF2a phosphorylation as a hotspot of stress-induced translation control. Out of the four mammalian eIF2a kinases, only GCN2 (general control non-derepressible 2) is conserved in plants[5, 6]. It is selectively stimulated by amino acid depletion in plants, fungi, and metazoan and is mandatory for pathogen-induced growth arrest via beta-aminobutyric acid[7–9]. The biogenesis of ribosomes is regulated in all eukaryotes by the highly conserved sensor–kinase TOR (target of rapamycin)[3, 10]. In addition to ribosome biogenesis, TOR controls cell-cycle progression, cell growth and autophagy in animals, yeast and plants, making TOR the master regulator of growth in autotrophic and heterotrophic eukaryotes[3, 11, 12]. In plants, TOR is known to balance growth with carbon availability by affecting brassinosteroid signaling[13] and to control life span[14]. It furthermore regulates translation re-initiation of uORF-containing mRNAs[15] and triggers stress responses by phosphorylation of its downstream target S6 kinase[16]. Xiong et al. coined the term glucose-TOR (Glc-TOR) signaling to describe control of TOR activity by glucose through glycolysis and mitochondrial bioenergetics to regulate meristem activation. Recent reviews describe the role of plant TOR in autophagy regulation, auxin sensing, development, and nutrient sensing[17–20].

In animals, TOR perceives systemic signals like growth factors and local signals like cellular energy load[3]. Amino acids are the most potent activators of TOR in animals[21, 22]. However, the established transducers of amino acid sensing to TOR in yeast and humans (the TOR-interacting proteins: RAG GTPase, TSC1/2, and RHEB) are absent in plants[23]. This raises the fundamental question if and how amino acid sensing is achieved in photoautotrophic organisms, which, in contrast to animals, are able to synthesize all proteinogenic amino acids due to assimilation of inorganic carbon (C), nitrogen (N), and sulfur (S).

In this study, we addressed the relevance of TOR for sensing of the amino acid cysteine in *Arabidopsis thaliana*. We focused on cysteine, since it is the central metabolite that coordinates the flux of sulfur with fluxes of carbon and nitrogen in all chemo-
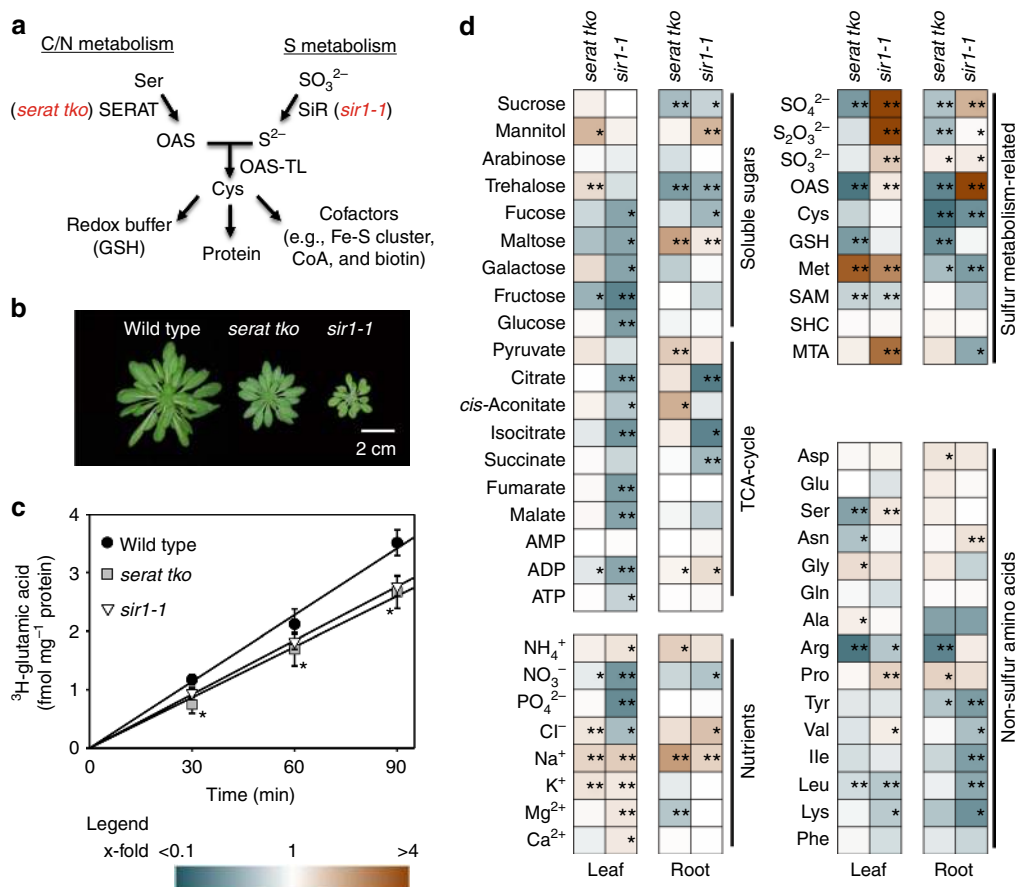

Fig. 1 Limitation of OAS or sulfide for Cys biosynthesis results in decreased translation and distinct metabolic phenotype. **a** Metabolic pathway of cysteine biosynthesis. **b** Rosette phenotype of 7-week-old wild-type *serat tko* and *sir1-1* grown in hydroponic culture. Scale bar, 2 cm. **c** Global translation rate in different genotypes as determined by time-resolved incorporation of ^{3}H-glutamic acid into proteins ($n = 3$, mean ± s.e.m., one-way ANOVA, $*p < 0.05$). **d** Relative fold change of metabolites is depicted as a heat map in cysteine-synthesis-depleted mutants compared to wild type ($n = 3$-4, one-way ANOVA, $*p < 0.05$, $**p < 0.01$)
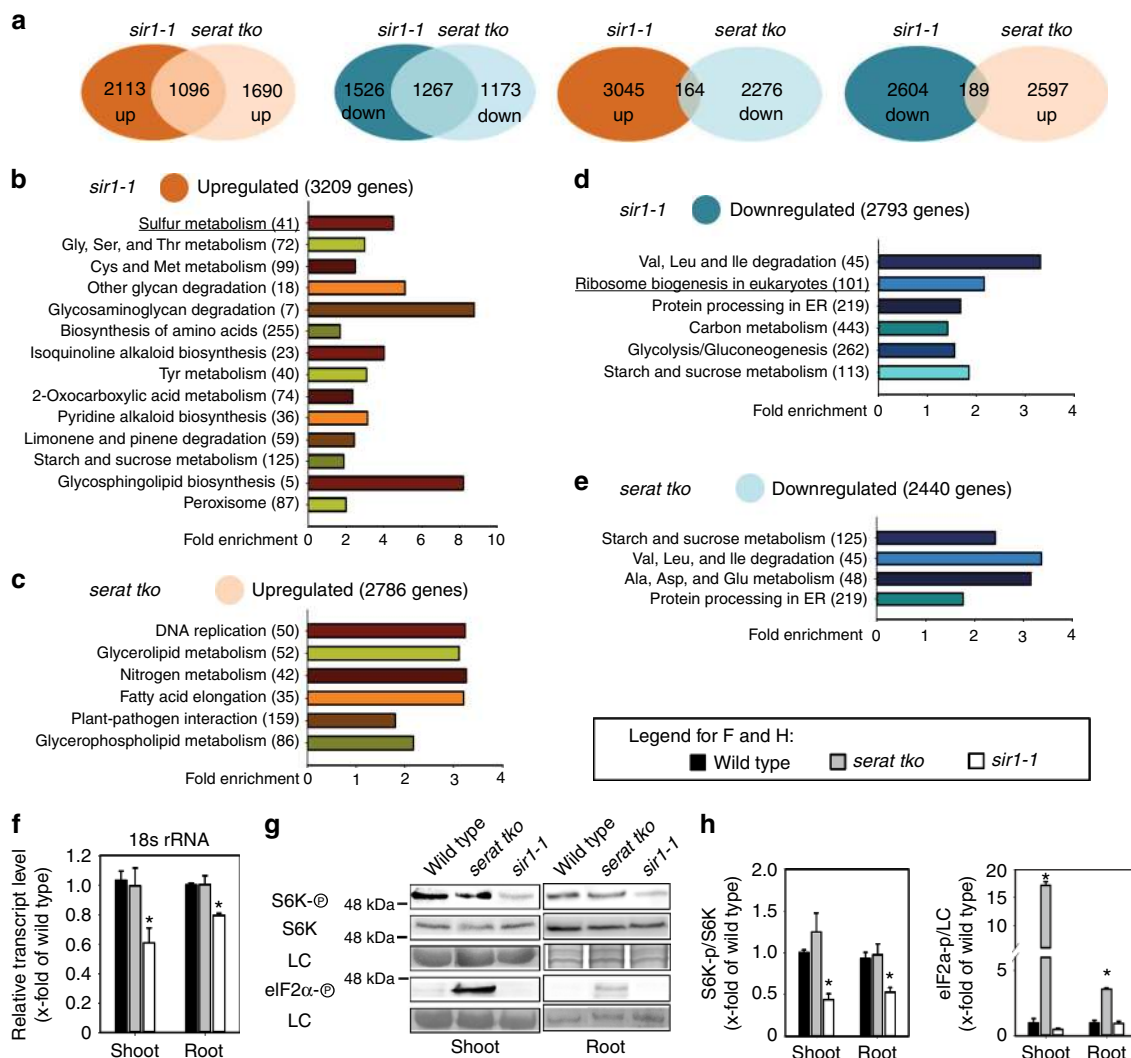
Fig. 2 Specific sensing of C/N- or S-precursors for Cys results in distinct transcriptome reprogramming and specific translation regulation. **a** Venn diagrams and **b–e** functional category analysis ($p < 0.05$, FDR < 0.25) for transcriptional response in roots of 7-week-old *serat tko* and *sir1-1* plants. The compared sets of genes contained transcripts, which were significantly ($p < 0.05$) up- or downregulated by more than 1.25-fold in *sir1-1* or *serat tko* in comparison to the wild type. The details of the highlighted categories with underlines are further presented in Supplementary Figs. 2 and 4. **f** Specific downregulation of 18s rRNA in response to sulfide limitation ($n = 3$, mean ± s.e.m., one-way ANOVA, $*p < 0.05$). **g** TOR and GCN2 activity was determined by antibodies against S6K-p, S6K (apparent sizes: 52 kDa) and eIF2α-p (apparent size: 43 kDa) and **h** calculated by the ratio of S6K-p/S6K and eIF2α-p/LC in x-fold of wild type ($n = 3$, mean ± s.e.m., one-way ANOVA, $*p < 0.05$)

autotrophic and photo-autotrophic organisms. Our results provide evidence that the availability of cysteine precursors, rather than cysteine itself, is sensed by plants. This unique mechanism allows plants to distinguish between limitations of carbon/nitrogen (C/N) vs. limitation of sulfur (S) for amino acid biosynthesis. Selective sensing of precursor limitations for cysteine synthesis is accomplished in the C/N branch by GCN2 or in the S branch by Glc-TOR signaling. The differential activation of both sensor kinases regulates meristematic activity, translation efficiency, inorganic sulfur uptake, and remobilization of nutrients by autophagy to coordinate growth with nutrient limitation. The data reveal a specific adaptation of the TOR system to the photo-autotrophic lifestyle of plants.

Results

Impact of sulfide or OAS supply on translation and growth.
Synthesis of the sulfur-containing amino acid cysteine by *O*-acetylserine-(thiol)lyase (OAS-TL) is the sole entry point of reduced sulfur in the form of sulfide into plant metabolism,

thereby coordinating the flux of sulfur with the fluxes of carbon and nitrogen[24]. Provision of sulfide by sulfite reductase (SiR) and the C/N precursor *O*-acetylserine (OAS) by serine acetyl-transferase (SERAT) are known to limit cysteine synthesis in plants[25–28] (Fig. 1a). In order to understand sensing of cysteine limitation in autotrophic eukaryotes, we used *Arabidopsis thaliana* to engineer a triple knockout plant (*serat tko*) that lacked the major SERAT isoforms in the cytosol (SERAT1;1), the plastids (SERAT2;1), and the mitochondria (SERAT2;2) and compared it to the *sir1-1* knock-down plant (Fig. 1b and Supplementary Fig. 1a). SERAT activity was unaffected in *sir1-1* and decreased to $5 \pm 2\%$ (mean ± s.e.m.) of wild-type level in *serat tko* (Supplementary Fig. 1b). The *sir1-1* mutation decreased SiR abundance to $8 \pm 4\%$ (mean ± s.e.m.) of wild-type level. The SiR abundance was enhanced in *serat tko* strongly suggesting that sulfide supply by SiR is not co-downregulated in this mutant (Supplementary Fig. 1c). Both mutants were impaired in cysteine synthesis and retarded in growth compared to wild type (Fig. 1b and Supplementary Fig. 1d). Significantly lowered translation of proteins as
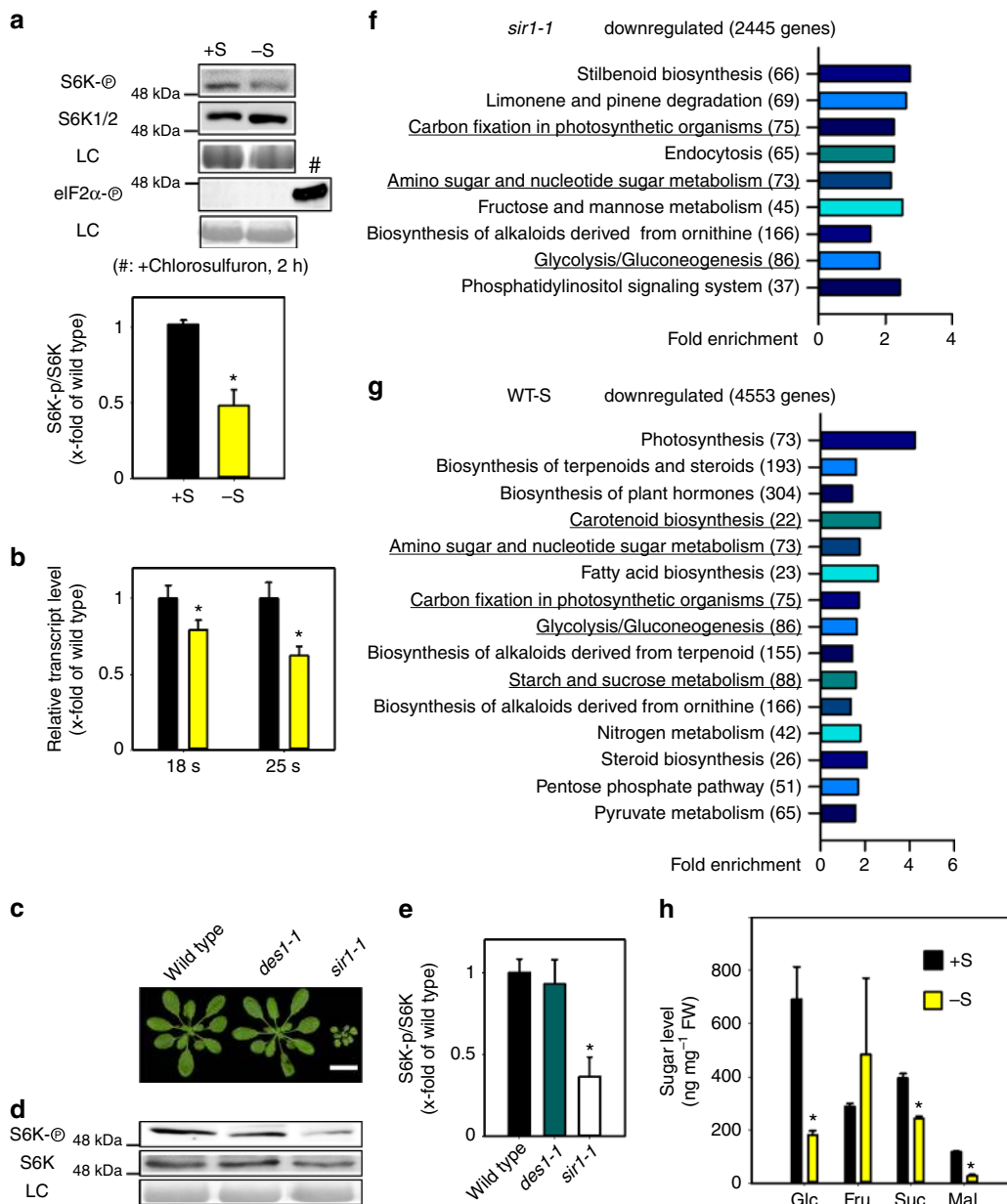
Fig. 3 Sulfur availability downregulates TOR activity and sugar metabolism. **a** Immunological detection of S6K-p, S6K (52 kDa) and eIF2α-p (43 kDa) with specific antisera was used for calculation of relative TOR activity by the ratio of S6K-p/S6K in x-fold of wild type ($n = 3$, mean ± s.e.m., t-test, $*p < 0.05$). **b** 18s and 25s rRNA level were measured in the shoot of wild type under sulfur deficiency ($n = 3$, mean ± s.e.m., t-test, $*p < 0.05$). **c** Growth phenotype of the *des1-1* mutant having low sulfide level in the cytosol. Scale bar, 2 cm. **d** Immunological detection of S6K phosphorylation status in the genotypes shown in **c** (apparent sizes of S6K-p, S6K: 52 kDa). **e** Calculation of TOR activity by the ratio of S6K-p/S6K in x-fold of wild type ($n = 3$, mean ± s.e.m., one-way ANOVA, $*p < 0.05$). **f**, **g** Functional category analysis ($p < 0.05$, FDR < 0.25) for downregulated genes in shoots of 7-week-old *sir1-1* and sulfur-deficient WT plants. The compared sets of genes contained transcripts, which were identified by microarray analysis to be significantly ($p < 0.05$) downregulated by more than 1.25-fold. The categories related to sugar metabolism are highlighted with underlines. **h** Soluble sugar levels in shoots of 7-week-old sulfur-deficient plants ($n = 4$, mean ± s.e.m., t-test, $*p < 0.05$)

determined by incorporation of glutamic acid into the total protein fraction in fully differentiated leaf cells was observed (Fig. 1c).

Limitation of sulfide or OAS triggers specific responses. Next, we measured metabolite levels in the respective mutants to study the metabolic consequences of impaired SERAT or SiR activity (Fig. 1d). Although both mutants suffered from impaired cysteine synthesis, they showed very different adaptions of primary metabolism due to limitation of either C/N precursor in *serat tko*

mutants or sulfide in *sir1-1* mutants. These specific adaptations occurred in photo-autotrophic (leaves) and heterotrophic tissue (roots) of both mutants, albeit to a different extent for individual compounds (Fig. 1d and Supplementary Fig. 1e). In *sir1-1*, the levels of several carbohydrates were downregulated, which in turn caused depletion of intermediates of the tricarboxylic acid (TCA) cycle in roots and leaves. Depletion of TCA cycle intermediates was not evident in *serat tko* and was corroborated by only marginally affected monosaccharide levels. Accordingly, the energy charge was specifically only lowered in shoots and roots of *sir1-1* plants (Supplementary Fig. 1f). These results indicate that carbon

fixation into glucose and use of glucose in the TCA cycle was not downregulated due to decreased cysteine biosynthesis, but specifically in response to lowered sulfur assimilation in *sir1-1*. OAS, the product of SERAT, and sulfate were decreased in leaves and roots of *serat tko* but accumulated in *sir1-1* in accordance with the known regulatory link between OAS and the high-affinity uptake system for sulfate[24]. Cysteine steady state levels were only depleted in heterotrophic roots but kept constant in leaves of both mutants. The unexpected finding of unchanged cysteine pools in leaves ruled out the possibility that decreased translation in both mutants is a simple consequence of lowered cysteine pool size. Obviously, both mutants specifically sensed decreased cysteine precursor supply and responded in both cases with decreased growth and decreased translation in order to maintain the cysteine steady state level in leaves.

Limitation of sulfide but not OAS decreases ribosomal RNA. To uncover the specific signaling mechanisms in response to C/N precursor limitation or S-precursor limitation for cysteine in both mutants, we performed microarray-based expression profiling. The analysis of global transcriptome changes in roots of *sir1-1* and *serat tko* revealed a specific response to OAS limitation for cysteine biosynthesis in *serat tko* and limited sulfur supply in *sir1-1* (Fig. 2a). An enrichment analysis of functional categories of the significantly regulated genes in *sir1-1* (Fig. 2b, c and Supplementary Tables 1 and 2) and *serat tko* (Fig. 2d, e and Supplementary Tables 1 and 2) uncovered several commonly downregulated pathways, including protein processing in the ER and branched-chain amino acid degradation. Downregulation of these pathways is in agreement with the observed decreased translation rate in both mutants (Fig. 1c). Specifically in *sir1-1*, sulfur metabolism was significantly upregulated (Fig. 2b). This included induction of the high-affinity sulfate transporters *SULTR1;1* and *SULTR1;2* and explained the strong accumulation of sulfate in *sir1-1* (Fig. 1d). The entire sulfur deficiency response (induction of sulfate uptake and sulfate reduction) was evidently absent in roots of *serat tko* (Supplementary Fig. 2 and Supplementary Table 2), which provides a functional explanation for the many differences observed in the metabolite fingerprints of both mutants (Fig. 1d and Supplementary Fig. 1e).

In roots of *sir1-1*, messenger RNAs (mRNAs) encoding for ribosome proteins and proteins associated with ribosome biogenesis accumulated to lower levels when compared to the wild type (Fig. 2c and Supplementary Fig. 3). The significant enrichment for downregulated transcripts related to ribosome biogenesis provides the most likely explanation for the decreased translation rate observed in *sir1-1* (Fig. 1c). Surprisingly, ribosome biogenesis was not affected in *serat tko*, although *serat tko* showed a similar phenotype to *sir1-1* with respect to slower growth and decreased translation (Fig. 1b, c).

TOR regulates translation in *sir1-1* but not in *serat tko*. The specific downregulation of transcripts related to ribosome biogenesis prompted us to test the abundance of the 18S and 25S rRNAs. Only in *sir1-1*, the abundances of these rRNAs were significantly decreased in shoots (18s rRNA: $61 \pm 10\%$, 25s rRNA: $60 \pm 2\%$, mean $\pm$ s.e.m.) and roots (18s rRNA: $79 \pm 2\%$, 25s rRNA: $53 \pm 7\%$, mean $\pm$ s.e.m., Fig. 2f and Supplementary Fig. 4). In plants, transcription of rRNAs and translation are under positive control of TOR[10, 15], which specifically phosphorylates the downstream kinase S6K at Thr[449] [3, 29]. This phosphorylation is the canonical trigger for activation of ribosome biogenesis and translation in eukaryotes[3]. When we assayed the phosphorylation of S6K with a phospho-specific antiserum, we found it to be decreased by $56 \pm 7\%$ in shoots and $47 \pm 6\%$ in roots of *sir1-1*. In

contrast, *serat tko* displayed wild-type-like S6K phosphorylation levels (Fig. 2g, h). In order to show the specificity of TOR downregulation by decreased SIR abundance, we tested two additional SiR mutants, KD1T (*sir1-3*) and KD3P (*sir1-4*) described in Yarmolinsky et al.[30]. The *sir1-3* mutant was retarded in growth due to significantly lowered SiR abundance, whereas *sir1-4* displayed wild-type-like phenotype and SiR protein level (Supplementary Fig. 5a–d). In line with the observed SIR abundance in both lines, TOR activity was only decreased in *sir1-3* but not in *sir1-4* (Supplementary Fig. 5d, e). These results suggest that significant downregulation of SiR in *sir1-1* and *sir1-3* causes downregulation of TOR activity as determined by phosphorylation of its downstream target S6K. Since *serat tko* plants have reduced translation rates (Fig. 1c) but neither reduced 18S rRNA levels (Fig. 2f) nor reduced TOR activity (Fig. 2h), we tested if the reduced global translation in *serat tko* is caused by phosphorylation of the eukaryotic initiation factor eIF2α. Immunological detection of eIF2α phosphorylation revealed 17 ± 1 (mean $\pm$ s.e. m.) fold more abundance of the phosphorylated eIF2α protein in leaves and 3.6 ± 0.1 (mean $\pm$ s.e.m.) fold more in roots of *serat tko* when compared to wild type. Phosphorylation of eIF2α was not affected in *sir1-1* (Fig. 2g, h).

In sum, *sir1-1* mutants and *serat tko* appear to reduce global translation rates via two independent sensing mechanisms: in *sir1-1* via downregulation of TOR, whereas in *serat tko* via elevated eIF2α phosphorylation.

Sulfur deficiency decreases TOR activity and glucose levels. In search for the molecular signal that triggers TOR inhibition after decreased S-precursor supply for cysteine biosynthesis in *sir1-1*, we characterized the impact of sulfate deprivation on TOR and GCN2 activity. Sulfate deficiency caused specific decrease of TOR activity in leaves of wild-type plants, whereas the stress-related sensor–kinase GCN2 was not affected (Fig. 3a and Supplementary Fig. 6a). In agreement with GCN2 not playing an important role in sulfate sensing, a GCN2 loss-of-function mutant was not more sensitive to sulfate deprivation and showed the same response as the wild type with respect to sulfur deficiency-induced metabolite adaptations (Supplementary Fig. 6b).

Inhibition of TOR by sulfate deprivation resulted in significantly lower amounts of 18S and 25S rRNA in the wild type (Fig. 3b). Impairment of sulfur reduction by sulfate deprivation in the wild type or by the *sir1-1* mutation could inhibit TOR by directly affecting the cytosolic sulfide concentration or by an unknown messenger. To test the first hypothesis, we determined TOR activity in the *des1-1* mutant, which has previously been shown to possess low sulfide levels in the cytosol[31]. In our growth conditions, *des1-1* grew like wild type and displayed TOR activity similar to wild type (Fig. 3c). In contrast, *sir1-1* produced less biomass, which is consistent with the lowered TOR activity in comparison to wild type and *des1-1* (Fig. 3d, e), making cytosolic sulfide levels an unlikely signal. In search for a potential messenger system that transmits the sulfide limitation signal from the chloroplasts to the cytosolic TOR sensor–kinase complex, we compared the transcriptional response of wild-type plants to sulfate deprivation with the transcriptional response of SiR-activity-depleted plants (*sir1-1*, Fig. 3f, g). We found that photosynthesis and several carbon metabolic routes are affected in the same way under both conditions (Fig. 3f, g and Supplementary Table 3). Furthermore, carbon metabolism and glycolysis was specifically downregulated in roots of *sir1-1* but not in roots of *serat tko* (Fig. 2c, e). In plants, carbohydrates are mainly produced in chloroplasts by de novo fixation of CO_2 via photosynthesis but transported into the cytosol for further metabolization. Since glucose (Glc) and its metabolization in
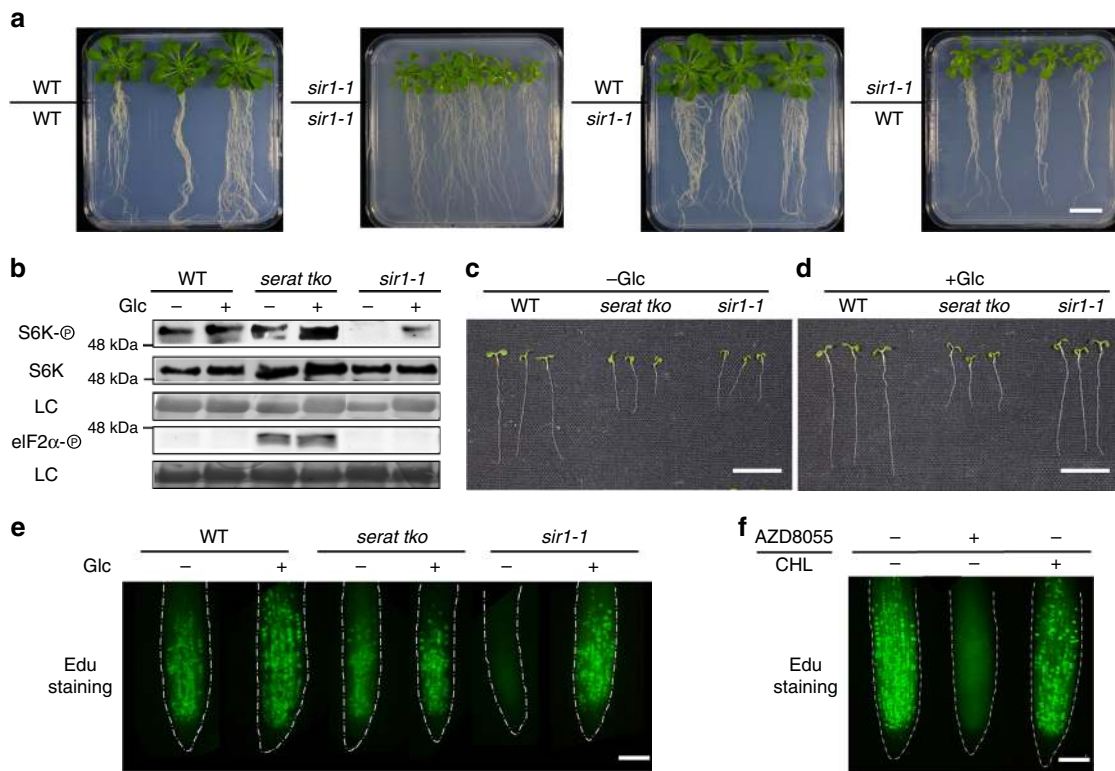
Fig. 4 Sulfur availability regulates root meristem and plant growth via glucose-TOR. **a** Phenotype of chimeric plants obtained by grafting of wild-type (WT) and sir1-1 organs. Identity of organs is depicted as shoot/root. Scale bar, 2 cm. **b–e** Feeding of serat tko and sir1-1 seedlings with glucose. **b** Immunological detection of S6K-p, S6K (apparent sizes: 52 kDa), and eIF2α-p (apparent size: 43 kDa) with specific antisera in wild-type serat tko and sir1-1. **c, d** Phenotype of wild-type serat tko and sir1-1 plants in the absence and presence of glucose. Scale bar, 1 cm. **e** Impact of glucose on root meristem activity in wild-type serat tko and sir1-1. Scale bar, 25 μm. **f** Root meristem activity of 7-day-old WT seedlings treated with TOR inhibitor (AZD-8055) or GCN2 activator (Chlorosulfuron, CHL) for 2 h. Scale bar, 25 μm

the TCA cycle is a well-established trigger of TOR in plants[11], we determined the most abundant carbohydrates in leaves of sulfate-deprived wild-type plants. Specifically Glc, maltose (Glc-Glc), and sucrose (Glc-Fru) were downregulated, while fructose (Fru) was unaffected (Fig. 3h). Also sir1-1 displayed a significant decrease of Glc and TCA cycle intermediates. Remarkably, Glc levels and TCA cycle intermediates were almost unaffected in serat tko (Fig. 1d).

Since limitation of sulfide supply by sulfate deprivation of the wild type or decreased SiR activity in sir1-1 resulted in decrease of soluble sugars and TOR activity, we analyzed TOR activity and sugar levels after short-term sulfide fumigation. Fumigation of sulfide for 6 h caused a strong increase of soluble sugars (Glc, Fru, Suc, and Mal) and TOR kinase activity (Supplementary Fig. 7), strongly indicating a positive correlation between sulfide level and soluble sugar level and TOR activity. Taken together, these results raise the possibility that reduced glucose metabolization provide the specific trigger for downregulation of TOR in sir1-1 and sulfur-deprived wild-type plants via the established glucose-TOR signaling[11].

Low glucose levels trigger inhibition of TOR in sir1-1. Roots and shoots of higher plants can independently produce sulfide and cysteine. In contrast, de novo fixation of carbon into carbohydrates is restricted to the shoot of plants. Grafting of sir1-1 shoots to wild-type roots induced a sir1-1-like growth phenotype in wild-type roots, although these roots have the capacity to produce sulfide. Vice versa, grafting of wild-type shoots to sir1-1 roots complemented the sir1-1 root phenotype (Fig. 4a and Supplementary Fig. 8). These results further strengthen the

hypothesis that downregulation of carbohydrate production in sir1-1 shoots is the signal for TOR inhibition and that it controls TOR activity in sir1-1 roots via phloem-mediated transport of sucrose as it has been suggested earlier for photosynthesis-induced TOR activation in roots[11]. Since grafting of sir1-1 roots to wild-type shoots did not cause decreased growth of leaves, a potential root-to-shoot signal generated by low cysteine levels in roots of sir1-1 is unlikely.

In order to provide direct functional evidence for the regulation of TOR by Glc in sir1-1, we fed Glc to both cysteine-synthesis-depleted mutants. As expected, Glc application increased TOR activity in sir1-1 significantly (Fig. 4b and Supplementary Fig. 9a). The enhanced TOR activity restored growth of shoot and of root and resulted in an almost wild-type-like phenotype of the Glc/Suc-treated sir1-1 seedling (Fig. 4c, d and Supplementary Fig. 9b). The dwarf growth of sir1-3 was also rescued by exogenous glucose feeding (Supplementary Fig. 9c, d). In contrast, the growth of serat tko was not affected by Glc application, since Glc did not affect eIF2α-phosphorylation (Fig. 4b).

TOR is an important regulator of stem cell activation in plants[32]. Consequently, meristematic activity of sir1-1 roots was found to be significantly lower when compared with wild type and serat tko, due to inhibition of TOR in sir1-1. Application of Glc or sucrose—the phloem-mobile shoot-to-root carrier of Glc—restored meristematic activity and thus provides a molecular explanation for the significant growth stimulation of Glc-treated sir1-1 seedlings (Fig. 4e and Supplementary Fig. 10a, b) that restored 87 ± 4% (mean ± s.e.m.) of biomass production by the wild type (Supplementary Fig. 8d). Glc-induced root
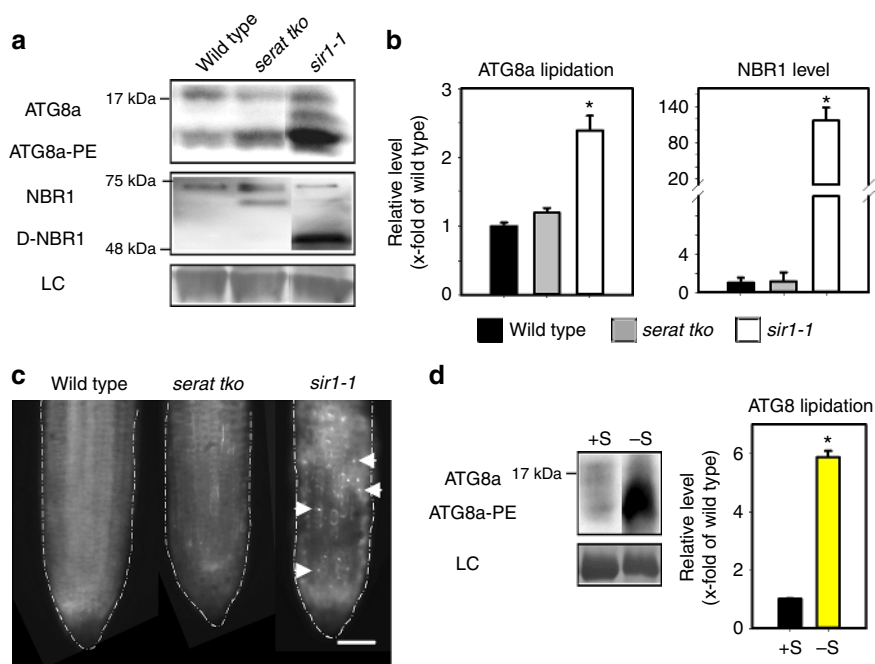
Fig. 5 Autophagy is specifically induced by limited S-precursor supply for cysteine biosynthesis. **a** Autophagy induction in the shoot of *serat tko* and *sir1-1* was determined by immunological detection of the canonical autophagy marker ATG8a and NBR1 with specific antisera. Lipidation of ATG8a (ATG8a-PE) (apparent size: 15–20 kDa) is essential for autophagosome formation and indicated by a significant shift during electrophoresis. NBR1 is a cargo receptor for selective autophagy and consequently degraded in autophagic bodies (D-NBR1) (apparent size: 50–75 kDa). **b** Level of ATG8a-PE and D-NBR1 shown in **a** were quantified ($n = 3$, mean $\pm$ s.e.m., one-way ANOVA, $*p < 0.05$). **c** Autophagy induction in the root of *serat tko* and *sir1-1* was detected by MDC staining. White arrows marked the visible autophagic bodies. Scale bar, 25 µm. **d** Autophagy induction in the shoot of WT under sulfur deficiency was determined by ATG8a-PE level ($n = 3$, mean $\pm$ s.e.m., *t*-test, $*p < 0.05$)

meristem reactivation in *sir1-1* was prevented by short-term inhibition of mitochondrial respiration or TOR activity (Supplementary Fig. 10c). In contrast, upregulation of eIF2α-phosphorylation in *serat tko* had no impact on meristematic activity (Fig. 4e). Also activation of GCN2 by chlorsulfuron application[8] did not affect root meristem activity (Fig. 4f and Supplementary Fig. 10d). In search for a TOR-independent functional explanation of the retarded growth phenotype of *serat tko*, we determined the cell size of wild-type *serat tko* and *sir1-1* and identified diminished cell elongation as a significant contributor to the smaller *serat tko* appearance (Supplementary Fig. 11).

Limited S supply for Cys synthesis induces autophagy. TOR is a well-established negative regulator of autophagy in metazoa, but its function in plants is less characterized[33]. Therefore, we treated Arabidopsis roots with the highly specific TOR inhibitor AZD-8055. Application of AZD-8055 caused a fast drop in phosphorylation of S6K and induced autophagy within 2 h, as demonstrated by lipidation of the autophagosome marker ATG8a (Supplementary Fig. 12a). The ribosomal RNA was decreased to $21 \pm 3\%$ of control level after 6 h of TOR inhibition (Supplementary Fig. 12b). The phosphorylation of eIF2α was unaffected for up to 6 h of AZD-8055 treatment (Supplementary Fig. 12a), which is in agreement with unchanged GCN2 activity in TOR overexpression and TOR-RNAi lines[8]. Since TOR is significantly downregulated in *sir1-1*, we tested if autophagy is also induced in this mutant. Lipidation of ATG8a (Fig. 5a, b), degradation of the selective autophagy cargo receptor neighbor of BRCA1 (NBR1, Fig. 5a, b) and fluorescent staining of acidic autophagosomes (Fig. 5c) demonstrated a significant upregulation of autophagy in *sir1-1* leaves and roots. Autophagy was not induced in *serat tko* plants. From these findings, we presumed that decrease of TOR activity by impairment of sulfate reduction might also trigger

autophagy induction under sulfate deprivation. Indeed, sulfate deficiency significantly induced autophagy in leaves of wild-type plants as shown by ATG8 lipidation (Fig. 5d). Taken together, these results uncover the importance of enhanced autophagy for remobilization of internal resources during sulfur deprivation and that the trigger for induction of autophagy under sulfur deprivation is the decreased TOR activity due to lowered S-precursor supply for cysteine biosynthesis.

Discussion

Eukaryotic cells invest significant resources in protein translation and have therefore established sophisticated mechanisms to regulate this process in response to growth stimuli and nutrient supply. In the heart of this regulation lies the sensor–kinase TOR. The most comprehensive signaling network of TOR is found in humans. It consists of two sensory protein complexes mTORC1 and mTORC2, which perceive signals from growth factors and diverse nutrient stimuli[34]. Direct sensing of amino acid levels via the Rag-TSC2-Rheb axis is one of the most important functions of TOR in humans[35]. This mechanism is largely conserved in fungi and orthologous proteins of this axis are present in opisthokonts[22, 36, 37]. In contrast, we show here that plants do not directly sense the concentration of the amino acid cysteine but the supply of its precursors. In plants as photo-autotrophic organisms, cysteine is the metabolic hub that integrates the products of reductive assimilation of sulfate, nitrate, and CO_2. The reason for the conceptually different approach of TOR function apparently is to allow plants to distinguish which building blocks from the S or the C/N assimilation pathways for cysteine synthesis are limiting and to respond in a highly specific manner to changing demands.

The absence of a direct cysteine-sensing mechanism is consistent with the previously observed lack of TOR activation

after application of an amino acid cocktail including cysteine[11]. It is remarkable in this context that the last common eukaryotic ancestor evidently possessed orthologs for RAG, TSC2, and Rheb[36], strongly indicating a specific loss of this signaling mechanism in the plant lineage of eukaryotes. Further plant-specific adaptions of the TOR signaling network are indicated by the absence of mTORC2 components in plants[36].

In search for the direct-sensing mechanism of the cysteine precursors, we identified GCN2 as the sensor for the supply via the C/N branch. This finding was unexpected due to the general role of GCN2 as an amino acid sensor in eukaryotes and the conserved mechanism from human to plants for activation of GCN2 by uncharged tRNAs[6, 9, 38]. However, GCN2 was not responding to sulfur limitation and decrease of cysteine levels in *sir1-1* roots, but was specifically activated by limitation of C/N supply for cysteine production by a so far unknown mechanism. Consequently, GCN2 did not contribute to regulation of the sulfur deficiency response.

The downregulation of TOR activity in the *sir1-1* mutant and during sulfur deficiency in the wild type demonstrated that the sensing of the precursor supply of the S branch takes place via this sensor–kinase. In search for the signal that links S-precursor supply with TOR activity, we observed that glucose feeding ameliorated the S-deficiency phenotype of *sir1-1* and that decreased flux through the sulfate assimilation pathway in *sir1-1* or sulfate-deprived wild type resulted in downregulation of glucose bioenergetics. Furthermore, short-term sulfide fumigation caused fast and significant upregulation of glucose levels and TOR activity. Indeed, regulation of plant TOR by glucose was previously reported and requires glucose metabolization by the TCA cycle[11]. This finding explains the failure of glucose to trigger meristem reactivation in *sir1-1* when mitochondrial respiration or TOR inhibitors were co-applied with glucose. In humans, low energy/glucose levels inhibit mTORC1 by activation of the AMP-activated kinase (AMPK), which in turn phosphorylates RAP-TOR (regulatory-associated protein of TOR)[39]. The plant AMPK homolog, SnRK1.1, is not responding to high AMP levels but is activated by low levels of trehalose-6-phosphate (Tre6P). Tre6P is synthesized from glucose and acts as a general carbon status signal in plants, since its concentration tightly follows glucose metabolization[40]. SnRK1.1 phosphorylates plant RAPTOR1B and its overexpression caused decreased phosphorylation of TOR substrates[41]. Consequently, the observed sulfur deficiency-induced low-glucose levels might have been sensed by SnRK1 that inhibited plant mTORC1 activity by phosphorylation of RAPTOR1B. Furthermore, short-term sulfide fumigation increases glucose levels and TOR activity, which is in agreement with the proposed role of the glucose-TOR signaling under sulfur deprivation. However, these data do not exclude a direct regulation of TOR by sulfide via a so far unknown mechanism.

The TOR-mediated response to sulfur deficiency included induction of autophagy for remobilization of internal resources, lowered translation, and inhibition of meristem activity. Many of these reactions have also been shown to occur upon deprivation of other nutrients, possibly suggesting a general role of TOR in nutrient sensing of plants. In particular, the control of meristem activity by nutrient availability is crucial, since developmental plasticity of the root system is a hallmark of many mineral nutrient-deficiency responses[42]. In line with the idea that TOR is a central regulator of meristem activity and consequently developmental plasticity in response to environmental cues, TOR has been evidenced recently to participate in the light-induced activation of the shoot apical meristem[32].

The surprising finding of differential activation of TOR and GCN2 by supply of distinct cysteine precursors provides the molecular framework for specific responses of plants toward diverse nutrient limitations and adds novel mechanistic insights into the homeostatic regulation of the macronutrient sulfur. We anticipate that the here-uncovered knowledge will stimulate research on regulation of other mineral nutrients and have profound impact on future breeding strategies to enhance nutrient use efficiency of crop plants, one of the currently most important traits of commercial breeding programs.

Methods

Plant genotypes and growth conditions. *Arabidopsis thaliana* mutant plants, as well as wild-type control plants were in the Columbia (Col-0) ecotype. Wild-type plants (N1092) and salk_103855 (des1-1) were gained from the Nottingham Arabidopsis Stock Centre. The triple-mutant *serat1;1 serat2;1* and *serat2;2* (*serat tko*) was constructed by crossing single *serat* T-DNA knock-out lines. The T-DNA insertion line *sir1-1* was described previously[25]. *sir1-3* (salk_075776, KD1T[30]) and *sir1-4* (sail_1223C03, KD3P[30]) were gained from Prof. Moshe Sagi (Weizmann Institute of Science, Israel). The *gcn2* mutant (GABI_862B02) was provided by Prof. Jean-Marc Deragon (University of Perpignan, France). If not otherwise indicated, plants were grown under short-day conditions for 2 weeks[25]. Then seedlings were transferred into larger pots containing 15 L half-strength Hoagland solution (pH 5.8) either supplemented with 500 μM MgSO$_4$ (normal sulfate condition) or 1 μM MgSO$_4$ (-S) for 5 weeks and were transferred to fresh media 24 h before being harvested. Glucose-feeding experiment was performed with seedlings grown on AT medium (pH 5.8, 0.6% agar) supplemented with 30 mM Glc. All plants were grown in a short-day climate chamber (8.5 h light/15.5 h dark; 80–100 μmol m^{-2}s^{-1}; 22 °C day/18 °C night; 50% humidity). Chemical inhibitor treatment was performed with media containing AZD-8055 (5 μM) or chlorosulfuron (0.5 μM) for 2 h.

Determination of translation. Leaf discs were incubated for 30, 60, and 90 min with radiolabeled 3H-glutamic acid (10 μCi ml^{-1}). After incubation, proteins were extracted and desalted using PD SpinTrap G-25 columns (GE Healthcare Life Science) to remove the non-incorporated ^{3}H-glutamic acid. To quantify incorporated radiolabeled glutamic acid into proteins, leaflets were dissolved in 10 ml scintillation liquid (Ultima Gold; Perkin Elmer) and counted for 5 min with the liquid scintillation analyzer Tri-Carb 2810TR (PerkinElmer).

Determination of metabolites. Soluble sugars were extracted by 80% ethanol and separated on Dionex ICS-3000 system with CarboPac PA1 with CarboPac PA1-Guard column at 25 °C. For the measurement of amino acids, thiols, and OAS, total metabolites were extracted from 50 mg leaf or root materials with 500 μl 0.1 M HCl. Determination of amino acids and OAS was based on the derivatization with the fluorescent dye AccQ-Tag™. An aliquot of 10 μl HCL extracts was mixed with 70 μl borate buffer (0.2 M, pH 8.8) and 20 μl 3 mg ml^{-1} AccQ-Tag™ solution. The derivatization was performed at 55 °C for 10 min. The separation of amino acids was performed by reversed phase HPLC on a Nova-Pak™ C18, 3.9 × 150 mm column. Derivatives were detected at an emission wavelength of 395 nm upon excitation at 250 nm. The data were analyzed using the software Empower Pro. To detect thiols, 25 μl HCl extracts were incubated with 245 μl reduction buffer (68 mM Tris, pH 8.3; 0.34 mM DTT; 25 μl 0.08 M NaOH) for 1 h at room temperature in the dark. Free thiol groups were released and derivatized with 0.85 mM MBB at room temperature for 15 min in the dark. An aliquot of 705 μl 5% acetic acid was used to stop the derivatization. The separation of thiols was performed by reversed phase HPLC on a Nova-Pak™ C18, 4.6 × 250 mm column. Thiol-bimane derivatives were detected at an emission wavelength of 480 nm upon excitation at 380 nm.

Ions were extracted from 50 mg materials in 300 μl ddH$_2$O. The extraction was carried out at 98 °C for 30 min under constant shaking. The aqueous extracts were diluted three times with ddH$_2$O to a final volume of 300 μl and transferred to HPLC vials (Dionex). The determination was carried out on a system ICS-3000 (Dionex) with an IonPac AS 11 column and 15–300 mM NaOH (Fluka, in ddH2O) as eluent. Quantitative calculation of the organic acids and ions was performed using Chromeleon software 6.7 (Dionex).

Immunological detection of proteins. For immunological detection of S6K-p and eIF2α-p, total soluble proteins were extracted from 50 mg plant materials with 250 μl 2× Laemmli buffer supplemented with 1% phosphatase inhibitor cocktail 2 (Sigma). Proteins were denatured for 5 min at 95 °C and separated on 10% SDS-PAGE. For immunological detection of S6K1/2, ATG8a-PE and NBR1, total proteins were extracted from 50 mg plant materials with 100 μl urea buffer (4 M urea, 100 mM DTT and 1% Triton X-100). Proteins were separated on 15% SDS-PAGE supplemented with 8 M urea. Subsequently, proteins were blotted to nitrocellulose membrane. The primary antibodies anti-S6k-p (Phospho-p70 S6 Kinase (p-Thr389), Cell Signaling, #9205, 1:5000), anti-S6K1/2 (Agrisera, #AS12-1855, 1:5000), eIF-2α Phospho (Epitomics, #1090-1, 1:10,000), anti-ATG8a-PE (Agrisera, #AS14-2811, 1:2000), and anti-NBR1 (Agrisera, #AS14-2805, 1:5000) were detected using the HRP-conjugated secondary antibody (1:30,000). The band

intensity was quantified by Image Quant LAS4000 version 1.21 and normalized by the loading control. Full scans of blots are presented in Supplementary Fig. 13.

Microarray analysis. Gene expression profiling was performed using an A. thaliana genechip (Aragene-1_0-st-typ) from Affymetrix (High Wycombe, UK). RNA was isolated from 100 mg homogenized leaf or root material of 7-week-old hydroponically grown plants with the peqGold total RNA Kit (Peqlab) according to the manufacturer's protocol. DNA digestion was performed with the peqGOLD DNase I Digest Kit (Peqlab). All further steps were conducted by the collaboration partner Core-Lab for microarray analysis (Centre for medical research (ZMF); University of Mannheim): Biotinylated antisense cRNA was prepared according to the Affymetrix standard labeling protocol. Hybridization on the chip was conducted on a GeneChip Hybridization oven 640, subsequently dyed in the GeneChip Fluidics Station 450 and thereafter scanned with a GeneChip Scanner 3000. The entire equipment set was provided by the Affymetrix-Company (Affymetrix, High Wycombe, UK).

Arrays were annotated using a custom CDF Version 17 with TAIR-IDs-based gene definitions. The raw fluorescence intensity values were normalized applying quantile normalization. Differential gene expression was analyzed based on log-linear mixed model ANOVA, using a commercial software package SAS JMP7 Genomics, version 6, from SAS (SAS Institute, Cary, NC, USA). A false-positive rate of $a = 0.05$ with FDR correction was taken as the level of significance. Functional category analysis by DAVID[43] was used to determine whether defined lists (or sets) of genes exhibit a statistically significant bias in their distribution within a ranked gene list (fold change cut: 1.25, $p < 0.05$, FDR < 0.25).

Determination of rRNA levels. Levels of rRNAs were detected by qRT-PCR after cDNA conversion with specific primers 18s rRNA_RT and 25s rRNA_RT (Supplementary Table 4) by RevertAid H-Minus First Strand cDNA Synthesis Kit (Fermentas). qRT-PCR was performed with Rotor-Gene SYBR Green PCR Kit (Qiagen) and primers listed in Supplementary Table 4 (detailed method in Supplementary Methods).

Determination of root meristem activity. Edu (5-ethynyl-2′-deoxyuridine) staining was performed using Click-iT® EdU AlexaFluor® 488 Imaging Kit (Invitrogen). Seven-day-old seedlings grown on AT medium (pH 5.8, 0.6% agar) supplemented with 30 mM Glc were transferred to AT medium supplemented with 30 mM Glc and 5 μM AZD-8055 or 0.5 μM chlorsulfuron for 2 h. Then 5 μl 1 μM EdU in liquid AT medium was added directly on the root tip. The root tips were incubated with EdU for 30 min in the climate chamber. Then the seedlings were fixed in 100 μl fixation/permeabilization reagent (4% formaldehyde, 0.1% Triton X-100 in 1× PBS) for 30 min. After fixation, seedlings were incubated in the dark with 100 μl Click-iT reaction cocktail (prepared according to the manufacturer's protocol, Click-iT® EdU AlexaFluor® 488 Imaging Kit, Invitrogen). The seedlings were washed with PBS buffer for two times. All the samples were analyzed by Leica DM IRB epifluorescent microscope with FITC/GFP filter (AlexaFluor 488: excitation 495 nm; emission 519 nm). Images were recorded by Leica DFC350 FX camera.

Micro-grafting. The grafting was performed with 7-day-old seedlings grown on ¼ MS media containing 1% sucrose, 1.4% agar, and 40 mg l⁻¹ ampicillin. Shoot and root stocks were grafted and fixed together in a silicon tube (0.3 mm diameter, 3 mm length). Survived grafted plants were kept in the same growth condition for 5 weeks.

MDC staining. Seven-day-old seedlings were incubated with 50 μM MDC (Monodansylcadaverine, Sigma) in PBS buffer (137 mM NaCl, 2.7 mM KCl, 10 mM Na_2HPO_4, 1.8 mM KH_2PO_4) for 15 min. Then the seedlings were washed with PBS buffer for two times and imaged by Leica DM IRB epifluorescent microscope with UV filter. Images were recorded by Leica DFC350 FX camera.

Data availability. Microarray data that support the findings of this study have been deposited in Gene Expression Omnibus database with the primary accession codes GSE93047, GSE93048, and GSE93049 (http://www.ncbi.nlm.nih.gov/geo/GSE93047). The authors declare that all other data supporting the findings of this study are available within the paper and its supplementary information files.

References

1. Lahtvee, P.-J., Seiman, A., Arike, L., Adamberg, K. & Vilu, R. Protein turnover forms one of the highest maintenance costs in Lactococcus lactis. *Microbiology* **160**, 1501–1512 (2014).

2. Munoz, A. & Castellano, M. M. Regulation of translation initiation under abiotic stress conditions in plants: is it a conserved or not so conserved process among eukaryotes? *Comp. Func. Genomics* **2012**, 406357 (2012).

3. Wullschleger, S., Loewith, R. & Hall, M. N. TOR signaling in growth and metabolism. *Cell* **124**, 471–484 (2006).

4. Browning K. S. & Bailey-Serres J. Mechanism of cytoplasmic mRNA translation. *Arabidopsis Book* **13**, e0176 (2015).

5. Zhang, Y. et al. GCN2-dependent phosphorylation of eukaryotic translation initiation factor-2α in *Arabidopsis*. *J. Exp. Bot.* **59**, 3131–3141 (2008).

6. Li, M. W., AuYeung, W. K. & Lam, H. M. The GCN2 homologue in *Arabidopsis thaliana* interacts with uncharged tRNA and uses Arabidopsis eIF2alpha molecules as direct substrates. *Plant. Biol.* **15**, 13–18 (2013).

7. Luna, E. et al. Plant perception of beta-aminobutyric acid is mediated by an aspartyl-tRNA synthetase. *Nat. Chem. Biol.* **10**, 450–456 (2014).

8. Lageix, S. et al. *Arabidopsis* eIF2alpha kinase GCN2 is essential for growth in stress conditions and is activated by wounding. *BMC Plant. Biol.* **8**, 134–142 (2008).

9. Howard, C. T. The metabolic sensor GCN2 branches out. *Cell Metab.* **5**, 85–87 (2007).

10. Kim, Y.-K. et al. Ribosomal protein S6, a target of rapamycin, is involved in the regulation of rRNA genes by possible epigenetic changes in *Arabidopsis*. *J. Biol. Chem.* **289**, 3901–3912 (2014).

11. Xiong, Y. et al. Glucose-TOR signalling reprograms the transcriptome and activates meristems. *Nature* **496**, 181–186 (2013).

12. Liu, Y. & Bassham, D. C. TOR is a negative regulator of autophagy in *Arabidopsis thaliana*. *PLoS ONE* **5**, e11883 (2010).

13. Zhang, Z. et al. TOR signaling promotes accumulation of BZR1 to balance growth with carbon availability in *Arabidopsis*. *Curr. Biol.* **26**, 1854–1860 (2016).

14. Ren, M. et al. Target of rapamycin signaling regulates metabolism, growth, and life span in Arabidopsis. *Plant Cell* **24**, 4850–4874 (2012).

15. Schepetilnikov, M. et al. TOR and S6K1 promote translation reinitiation of uORF-containing mRNAs via phosphorylation of eIF3h. *EMBO J.* **32**, 1087–1102 (2013).

16. Mahfouz, M. M., Kim, S., Delauney, A. J. & Verma, D. P. Arabidopsis TARGET OF RAPAMYCIN interacts with RAPTOR, which regulates the activity of S6 kinase in response to osmotic stress signals. *Plant Cell* **18**, 477–490 (2006).

17. Schepetilnikov, M. & Ryabova, L. A. Auxin signaling in regulation of plant translation reinitiation. *Front. Plant Sci.* **8**, 1014 (2017).

18. Pu, Y., Luo, X. & Bassham, D. C. TOR-dependent and -independent pathways regulate autophagy in *Arabidopsis thaliana*. *Front. Plant Sci.* **8**, 1204 (2017).

19. Baena-González, E. & Hanson, J. Shaping plant development through the SnRK1–TOR metabolic regulators. *Curr. Opin. Plant Biol.* **35**, 152–157 (2017).

20. Dobrenel, T. et al. TOR signaling and nutrient sensing. *Annu. Rev. Plant Biol.* **67**, 261–285 (2016).

21. Hara, K. et al. Amino acid sufficiency and mTOR regulate p70 S6 kinase and eIF-4E BP1 through a common effector mechanism. *J. Biol. Chem.* **273**, 14484–14494 (1998).

22. Li, L. & Guan, K. L. Amino acid signaling to TOR activation: Vam6 functioning as a Gtr1 GEF. *Mol. Cell* **35**, 543–545 (2009).

23. Rexin, D., Meyer, C., Robaglia, C. & Veit, B. TOR signalling in plants. *Biochem. J.* **470**, 1–14 (2015).

24. Takahashi, H., Kopriva, S., Giordano, M., Saito, K. & Hell, R. Sulfur assimilation in photosynthetic organisms: molecular functions and regulations of transporters and assimilatory enzymes. *Annu. Rev. Plant Biol.* **62**, 157–184 (2011).

25. Khan, M. S. et al. Sulfite reductase defines a newly discovered bottleneck for assimilatory sulfate reduction and is essential for growth and development in *Arabidopsis thaliana*. *Plant Cell* **22**, 1216–1231 (2010).

26. Heeg, C. et al. Analysis of the *Arabidopsis* O-acetylserine(thiol)lyase gene family demonstrates compartment-specific differences in the regulation of cysteine synthesis. *Plant Cell* **20**, 168–185 (2008).

27. Haas, F. H. et al. Mitochondrial serine acetyltransferase functions as a pacemaker of cysteine synthesis in plant cells. *Plant Physiol.* **148**, 1055–1067 (2008).

28. Wirtz, M. et al. Mitochondrial cysteine synthase complex regulates O-acetylserine biosynthesis in plants. *J. Biol. Chem.* **287**, 27941–27947 (2012).

29. Xiong, Y. & Sheen, J. The role of target of rapamycin signaling networks in plant growth and metabolism. *Plant Physiol.* **164**, 499–512 (2014).

30. Yarmolinsky, D., Brychkova, G., Fluhr, R. & Sagi, M. Sulfite reductase protects plants against sulfite toxicity. *Plant Physiol.* **161**, 725–743 (2013).

31. Álvarez, C. et al. Cysteine-generated sulfide in the cytosol negatively regulates autophagy and modulates the transcriptional profile in *Arabidopsis*. *Plant Cell* **24**, 4621–4634 (2012).

32. Pfeiffer, A. et al. Integration of light and metabolic signals for stem cell activation at the shoot apical meristem. *elife* **5**, e17023 (2016).

33. Liu, Y. & Bassham, D. C. Autophagy: pathways for self-eating in plant cells. *Annu. Rev. Plant Biol.* **63**, 215–237 (2012).

34. Kennedy Brian, K. & Lamming Dudley, W. The mechanistic target of rapamycin: the grand conducTOR of metabolism and aging. *Cell Metab.* **23**, 990–1003 (2016).

35. Demetriades, C., Doumpas, N. & Teleman, A. A. Regulation of TORC1 in response to amino acid starvation via lysosomal recruitment of TSC2. *Cell* **156**, 786–799 (2014).

36. Roustan, V., Jain, A., Teige, M., Ebersberger, I. & Weckwerth, W. An evolutionary perspective of AMPK–TOR signaling in the three domains of life. *J. Exp. Bot.* **67**, 3897–3907 (2016).

37. Binda, M. et al. The Vam6 GEF controls TORC1 by activating the EGO complex. *Mol. Cell* **35**, 563–573 (2009).

38. Dong, J., Qiu, H., Garcia-Barrio, M., Anderson, J. & Hinnebusch, A. G. Uncharged tRNA activates GCN2 by displacing the protein kinase moiety from a bipartite tRNA-binding domain. *Mol. Cell* **6**, 269–279 (2000).

39. Gwinn, D. M. et al. AMPK phosphorylation of raptor mediates a metabolic checkpoint. *Mol. Cell* **30**, 214–226 (2008).

40. Tsai, A. Y. L. & Gazzarrini, S. Trehalose-6-phosphate and SnRK1 kinases in plant development and signaling: the emerging picture. *Front. Plant Sci.* **5**, 119 (2014).

41. Nukarinen, E. et al. Quantitative phosphoproteomics reveals the role of the AMPK plant ortholog SnRK1 as a metabolic master regulator under energy deprivation. *Sci. Rep.* **6**, 31697 (2016).

42. Gruber, B. D., Giehl, R. F. H., Friedel, S. & von Wirén, N. Plasticity of the *Arabidopsis* root system under nutrient deficiencies. *Plant Physiol.* **163**, 161–179 (2013).

43. Huang, D. W., Sherman, B. T. & Lempicki, R. A. Systematic and integrative analysis of large gene lists using DAVID bioinformatics resources. *Nat. Protoc.* **4**, 44–57 (2009).

Acknowledgements

Author contributions

Additional information